ACS APPLIED MATERIALS & INTERFACES

Research Article

Cite This: ACS Appl. Mater. Interfaces 2017, 9, 43449−43458

www.acsami.org

Shear-Thinning and Thermo-Reversible Nanoengineered Inks for 3D Bioprinting

Scott A. Wilson,[†] Lauren M. Cross,[†] Charles W. Peak,[†] and Akhilesh K. Gaharwar*[,†,‡,§]

[†]Department of Biomedical Engineering, [‡]Department of Material Sciences, and [§]Center for Remote Health Technologies and Systems, Texas A&M University, College Station, Texas 77843, United States

ABSTRACT: Three-dimensional (3D) printing is an emerging approach for rapid fabrication of complex tissue structures using cell-loaded bioinks. However, 3D bioprinting has hit a bottleneck in progress because of the lack of suitable bioinks that are printable, have high shape fidelity, and are mechanically resilient. In this study, we introduce a new family of nanoengineered bioinks consisting of kappa-carrageenan (κCA) and two-dimensional (2D) nanosilicates (nSi). κCA is a biocompatible, linear, sulfated polysaccharide derived from red algae and can undergo thermo-reversible and ionic gelation. The shear-thinning characteristics of κCA were tailored by nanosilicates to develop a printable bioink. By tuning κCA−nanosilicate ratios, the thermo-reversible gelation of the bioink can be controlled to obtain high printability and shape retention characteristics. The unique aspect of the nanoengineered κCA−nSi bioink is its ability to print physiologically-relevant-scale tissue constructs without requiring secondary supports. We envision that nanoengineered κCA−nanosilicate bioinks can be used to 3D print complex, large-scale, cell-laden tissue constructs with high structural fidelity and tunable mechanical stiffness for regenerative medicine.

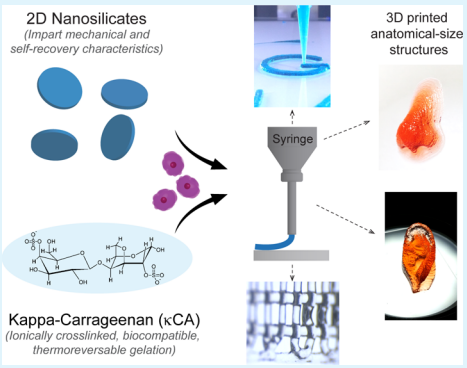

KEYWORDS: *nanocomposites, hydrogels, 3D bioprinting, two-dimensional (2D) nanoparticles, bioinks*

INTRODUCTION

Shear-thinning hydrogels are promising candidates for three-dimensional (3D) bioprinting because of their non-Newtonian behavior and stress−relaxation properties.[1−4] Hydrogel-based bioinks have been used to print cells in complex patterns for biomedical applications because of their biocompatibility and ability to recapitulate the extracellular matrix.[5,6] Some of the most commonly used polymers in bioprinting include alginate,[7,8] gelatin methacrylate (GelMA),[9,10] poly(ethylene oxide/glycol),[11] hyaluronic acid (HA),[12] and agarose.[13,14] Both alginate and agarose individually hold additional promise because of the high viscosities they can achieve, demonstrating high resiliency to the printing process.[13,15] These and other highly viscous polymers are often incorporated in blended bioinks as they can increase the printability of more bioactive but less-printable polymers, such as gelatin, GelMA, HA, and fibrinogen.[15−19] However, hydrogel-based bioinks still have limited shape fidelity after printing, low mechanical strength, and lack the ability to fabricate large-scale and self-supporting tissue constructs.[20−25]

To address this critical need, advanced bioinks are designed as rapidly gelling, shear-thinning hydrogel composites.[4,26] However, these bioinks often require support baths, photo-cross-linking, or post-processing that can add complexity to the print, lead to cell death, and produce mechanically weak constructs.[27−29] Thus, there is a critical need to develop new bioinks with shear-thinning characteristics, high print fidelity, tunable mechanical strength, high cell viability, and the ability to print anatomical-scale structures.

Here, we report a new family of shear-thinning and thermo-reversible bioinks from kappa-carrageenan (κCA) and nanosilicates (nSi or Laponite XLS) (Figure 1). κCA is a linear sulfated polysaccharide derived from red algae with alternating 3,6-anhydro-D-galactose and β-D-galactose-4-sulphate repetitive units.[30] This natural polymer has previously shown to be not only biocompatible, but also a viscous aid that is able to undergo quick thermo-reversible and ionic gelation, as well as a shear-thinning material at higher concentrations in solution.[31,32] When κCA is heated and dissolved in water, it presents a random coil structure; upon subsequent cooling, double helices (junctions) are formed due to hydrogen bonding between galactose units on the polymer backbone.[33] This thermo-reversible gelation can then be further stabilized by ionic cross-linking through positive ions, such as potassium (K^+), with κCA's negatively charged sulfate groups.[34] Compared to other positive ions, K^+ has shown to interact most synergistically with κCA to produce strong gels.[34] Despite interesting shear-thinning properties and gelation characteristics, κCA-based hydrogels have not been explored for 3D printing applications. By incorporating nSi within κCA hydrogels, we aim for a 3D print design with high fidelity.

Received: September 8, 2017
Accepted: November 6, 2017
Published: December 7, 2017

DOI: 10.1021/acsami.7b13602
ACS Appl. Mater. Interfaces 2017, 9, 43449−43458

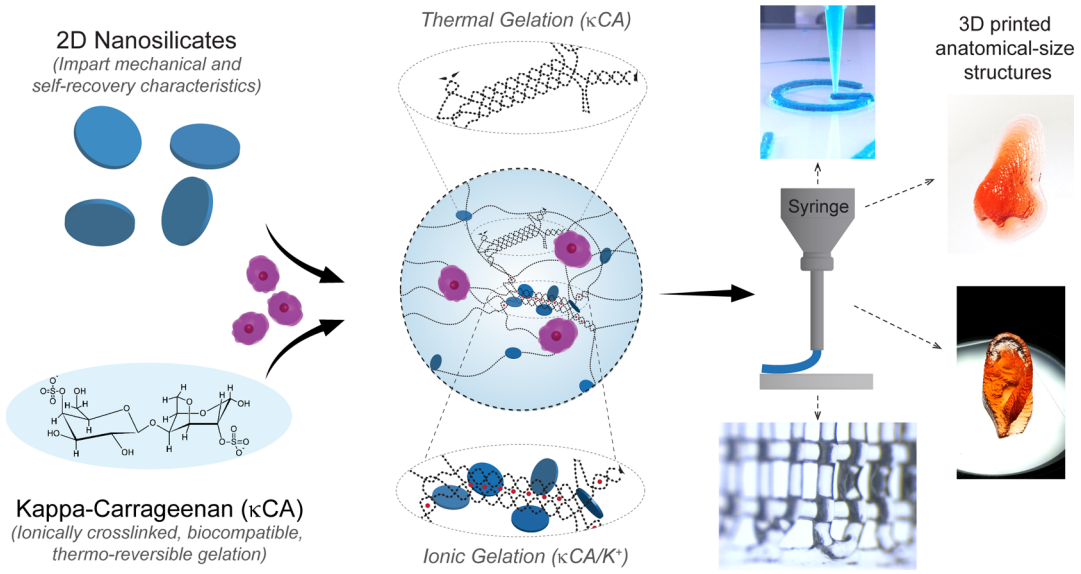

Figure 1. Synthesis of thermo-responsive and shear-thinning bioinks from nSi and κCA. Schematic showing the dual cross-linking process of thermo-reversible gelation and ionic gelation of the κCA network. Nanosilicate-stabilized cross-linked network due to physical interactions with κCA and ions to improve the mechanical stability of 3D-printed anatomical-size structures.

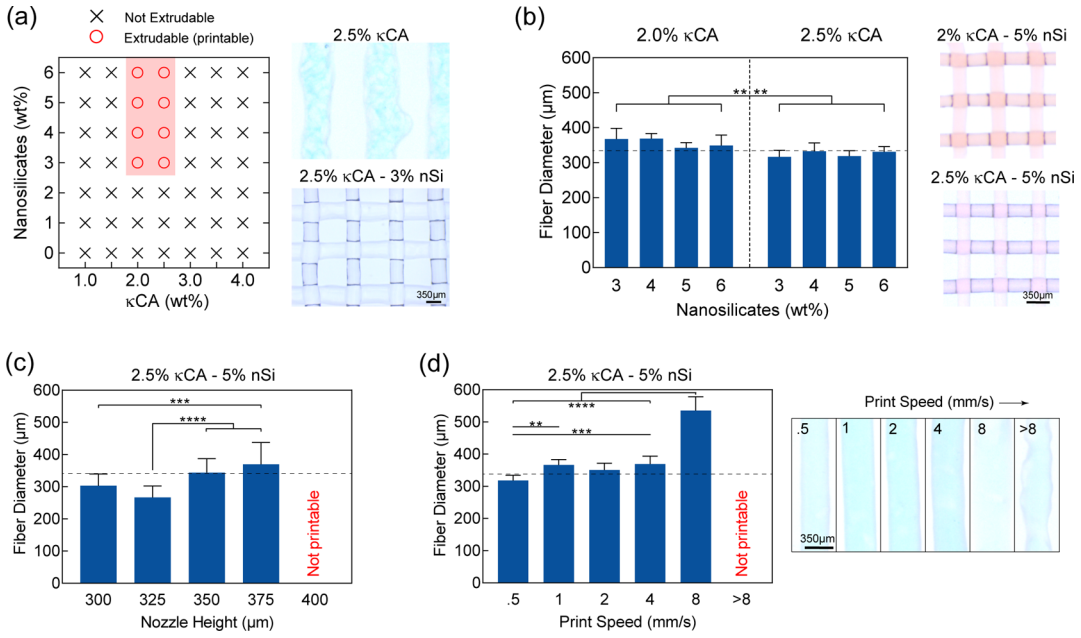

Figure 2. Optimizing κCA–nanosilicate ink processing and printing parameters. (a) Graph representing the printability of pure κCA and κCA–nanosilicate compositions. Corresponding images exhibit the difference that the addition of nSi has on the fiber diameter. (b) Different ink formulation show significant difference in the extruded fiber diameter while retaining high print fidelity. The dotted line represents printing nozzle diameter (337 μm of 23-gauge needle). (c) Change in nozzle height affects the size of the fiber diameter. (d) κCA–nanosilicate bioinks can be printed at a variety of speeds (up to 8 mm/s).

Nanosilicates (Laponite XLS) are two-dimensional (2D) synthetic silicates of low heavy-metal content and with 20–30 nm in diameter and 1–2 nm in thickness.[35−37] Because of their disc shape and high surface area, nanosilicates physically interact with the polymeric backbone and result in enhanced mechanical properties of polymeric networks.[37−42] These nanosilicates are dispersed using an inorganic polyphosphate dispersing agent to shield the positive charge on the edge of the nanoparticles. The negatively charged surfaces of nanosilicates allow for suspension in water at high concentrations without premature gelation. We propose to leverage this unique ability of nanosilciates (LAponite XLS) for enhanced control over the 3D printing process as there are no positive charges on nanosilicates to interact with anionic κCA.

In this report, we investigate the interactions between nanosilicates and κCA and optimize the composition of inks for 3D bioprinting. Specifically, we examine the effect of nanosilicates on shear-thinning and thermo-responsive characteristics of bioinks. We then tailor these interactions for printing anatomical-scale complex constructs with high shape fidelity and resolution. Finally, we evaluate in vitrothe biocompatibility of bioinks using mammalian cells. We envision that κCA–nSi

DOI: 10.1021/acsami.7b13602
ACS Appl. Mater. Interfaces 2017, 9, 43449–43458

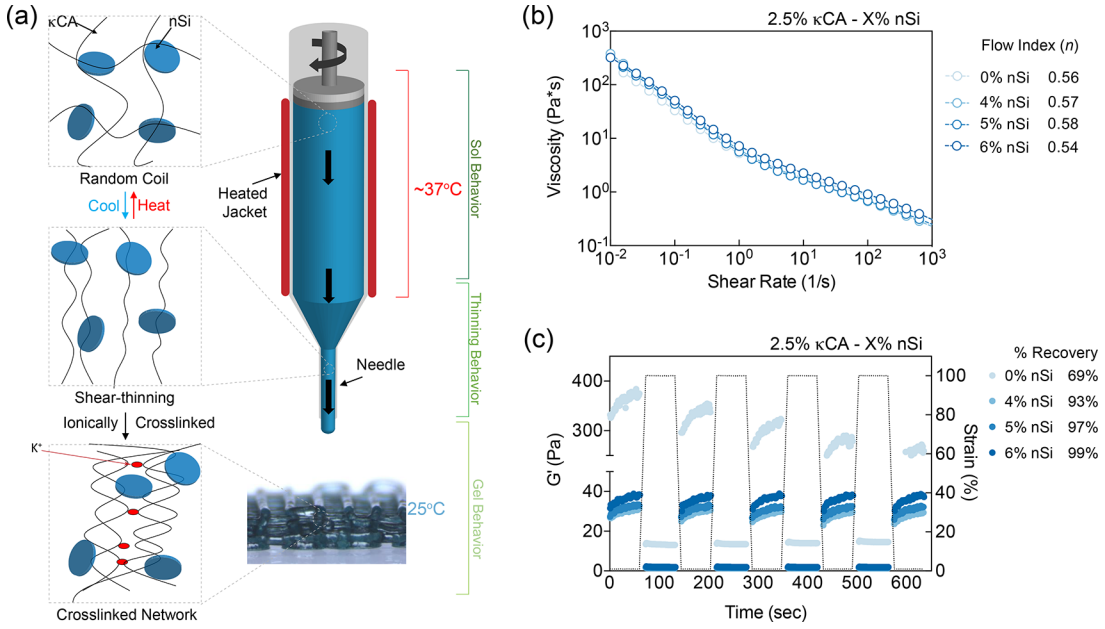

Figure 3. A schematic of κCA's coil-to-helix transition and material properties during the bioprinting process. (a) κCA undergoes thermo-reversible gelation upon heating and cooling which results in the formation of double-helical structures that can then be ionically cross-linked with the introduction of K^+ ions to form a stable network. (b) Shear rate sweep revealing the shear-thinning nature of κCA and κCA−nanosilicate bioinks. (c) Time sweep at 37 °C demonstrating percent recovery of bioink's storage modulus with the introduction of nSi.

bioinks can be used to print complex, large-scale, cell-laden constructs for regenerative medicine.

RESULTS AND DISCUSSION

Shear-Thinning and Thermo-Reversible Characteristics of κCA−Nanosilicate Bioinks. A key characteristic of bioinks is the ability of the material to be continuously extruded using a printing needle. To design bioinks, we first evaluated the printability of κCA and κCA−nSi nanocomposites by using an extrusion test. The extrusion tests were performed by pouring κCA and κCA−nanosilicate solutions into syringes and extruding using a syringe pump (Figure 2a). If the material could be continuously extruded without premature gelation and with minimal spreading after extrusion, it was deemed extrudable. We investigated the effect of κCA (1−4 wt %) and nanosilicate (0−6 wt %) concentrations on the ability of the gel to be extruded. The lower concentrations (1−1.5 wt %) of κCA were low-viscosity fluids and were not able to retain an extruded shape at 40 °C. This might be due to high polymer-chain mobility at low κCA concentrations that may prevent gelation because of limited chain interactions. With an increase in the κCA concentration, it is expected to reach a critical solution concentration that results in the formation of a viscous gel.

At a critical concentration of κCA, there will be enough galactose units interacting with other galactose units on the polymer chains, resulting in a physically entangled network because of hydrogen bonding between chains.[33] The observed low viscosities were similar to previous work investigating the critical gelation point of κCA, with a critical gel concentration being calculated at 1.9 wt % κCA at 40 °C.[43] From room temperature observations, higher concentrations (2−4 wt %) of κCA were highly viscous solutions. To disrupt hydrogen bonding, the solutions must be heated to 60 °C for extrusion. Upon extrusion of 2−4 wt % κCA, shape retention was low, and a high amount of spreading was observed. With time, the solution regained its viscosity; however, it is difficult for 3D printing. Although the extrusion bed temperature could be controlled to allow for faster gelation of κCA, tight temperature controls are necessary for cell bioprinting. On the basis of the extrusion test, we selected 2 and 2.5 wt % κCA as printable formulations.

The compositions of 2 and 2.5 wt % κCA with 3−6 wt % nSi had good shape retention and did not undergo premature gelation. This might be due to the addition of nSi, which allows additional sites for hydrogen bonding with the polymer backbone; which imparts shape retention, and also disrupts the polymer−polymer interactions of κCA to the thermo-reversible gel even at high concentrations. On the basis of these extrusion results, 2 and 2.5 wt % κCA were chosen as optimal polymer concentrations when used with 3−6 wt % nSi for 3D printing. The improvement in the printability of κCA with the addition of nSi can been seen in shape retention of the extruded filament using the bioprinter (Figure 2a). Shape retention elucidates if a material can be printed, whereas optimization of resolution, print fidelity, and shape retention after 3D printing can determine the applications in which the material can be used.

To mimic the native tissue architecture using 3D micro-extrusion printing, it is important to evaluate the resolution of the bioink. The control over printing parameters and material selection has a significant effect on the resolution of printed constructs. A typical resolution of extruded fibers ranges from 150 μm to 1 mm.[44] We investigated the effect of κCA (2 and 2.5 wt %) and nanosilicate (3, 4, 5, and 6 wt %) concentration on the printing resolution (Figure 2b). When using high-viscosity shear-thinning materials, it has been observed that increasing the polymer concentration can increase the printed resolution of the bioink.[8,13,19,45] Increasing the polymer concentration allows for enhanced polymer−polymer interactions to occur between polymer chains, which in turn can enable the bioink to have greater shape retention after it is

DOI: 10.1021/acsami.7b13602
ACS Appl. Mater. Interfaces 2017, 9, 43449−43458

printed. We believe that by increasing the concentration of κCA, we increased the amount of available interaction sites for hydrogen bonding between κCA polymer chains which led to an enhanced resolution. The resolution was further quantified, revealing that the 2 and 2.5 wt % κCA group's average fiber diameters were significantly different (p value < 0.0001) from each other; specifically, the 2.5 wt % κCA had a higher average resolution (325 ± 8.4 μm) than 2.0 wt % (357 ± 13.3 μm). As increasing the κCA concentration exhibited an increase in the resolution, we continued to use the 2.5 wt % κCA and 6 wt % nanosilicate formulation to optimize the printing parameters of the printing system.

Print speed and the nozzle to print bed height are two parameters that have been reported to influence printing resolution.[12,46] If the nozzle is too far from the print bed or if the print speed is too high, this can result in inconsistent deposition of fibers. In addition, finding the closest print height that matches the height of the deposited fibers is imperative to fabricating large constructs without delamination of layers. The distance of the nozzle from the print platform was investigated, and it was determined that a height of 350 μm allowed for the closest fiber diameter (343 ± 43 μm) relative to the needle size (337 μm) (Figure 2c). At a smaller nozzle height (300 and 325 μm), the printed fiber had a significantly lower diameter compared to the needle size. At a nozzle height of 400 μm, the material was not able to be deposited on the print bed. Printing at 350 μm provides a high resolution (similar size of the needle and the printed structure) and allows for close deposition of fibers. This close deposition of fibers is imperative to reducing the delamination of printed layers, which in turn leads to more mechanically robust constructs. Additionally, print speed is important for cell survival; the less time taken to print can increase cell survival, especially when fabricating larger constructs (Figure 2d).[44] There is also a tradeoff between print speed and resolution; lower speeds can produce higher resolutions because of the material having more time to gel. Above the highest speed of 8 mm/s, the bioink was not printable, having an inconsistent fiber diameter. However, the fiber resolution was still high (535 ± 43 μm) even at 8 mm/s speeds. For further testing, we chose 4 mm/s as it had a higher resolution (369 ± 25 μm) than 8 mm/s while remaining fast for printing larger constructs. By optimizing the material selection and printing parameters of the bioink and the bioprinter, we synthesized a bioink with high shape fidelity, resolution, and retention. We further evaluated bioinks containing 2.5 wt % κCA with different nanosilicate concentrations (4, 5, and 6 wt %) to print complex structures.

κCA−Nanosilicate Interactions during 3D Printing. During printing, the κCA−nanosilicate bioink is subjected to static and dynamic environments (Figure 3a). Initially, κCA exhibits a random coil structure that becomes aligned and elongated under shear; then upon cooling, the material displays a double-helix structure, that is further stabilized by ionic cross-linking.[33] κCA's material properties can be grouped into sol, shear-thinning, and gel behavior during the printing process. From these regions, we explored the effect of the nanosilicate addition on κCAs' ability to flow under shear force and recover from flow deformation.

Low-viscosity materials can be used for printing but have the observable limitation of shape fidelity after printing, which necessitates the use of highly viscous materials that are shear-thinning.[28] One model that mathematically describes shear-thinning fluids is the power-law equation ($\eta = K\dot{\gamma}^{(n-1)}$), where η is viscosity, $\dot{\gamma}$ is the shear rate, n is the flow index, and K is the consistency index. Flow index (n) describes a material's ability to thicken, thin, or remain Newtonian. A flow index (n) of less than one indicates a shear-thinning material, and this can be observed with a noticeable decrease in viscosity when there is an increase in the shear rate (Figure 3b).[47] κCA and κCA−nSi were observed to have similar shear-thinning characteristics, as quantified by the power-law flow index numbers of 0.56, 0.57, 0.58, and 0.54 for 0, 4, 5, and 6 wt % nSi, respectively. These values could indicate that nSi had no strong effect on κCA's shear-thinning ability and did not significantly disrupt κCA's polymer junction's ability to align when subjected to continuous shear. Measurements of κCA's flow behavior index indicated that κCA had a greater shear-thinning ability than commonly used polymers for bioink blends, such as alginate. Previous reports have indicated a flow behavior index of 0.90 for 2.25 wt % alginate compared to the observed 0.56 for κCA in the present study.[48,49] This shear-thinning behavior indicates how the material will react in a dynamic environment which prefaces the final static environment the κCA−nanosilicate bioink will experience after printing.

The effect of nSi on recovery was investigated by subjecting the bioink precursor solutions to low (1%) and high (100%) strain percentages. During the printing process, the bioink is subjected to different degrees of strain before it is printed and must be deformable and able to reform many times while retaining its mechanical properties. In addition, percent recovery from strain is also an indication of shape retention after printing which can therefore affect the mechanical properties of the printed constructs. It was observed that κCA's storage modulus (G') significantly decreased, from 360 ± 15 to 249 ± 15 Pa, when subjected to alternating high (100%) and low (1%) strains, presenting a low percent recovery of its G' (69%) (Figure 3c). Importantly, all nanosilicate compositions exhibited high percent recovery of G', with 6 wt % nSi having a percent recovery of 99%. In addition, the time required to recover the network property after cessation of shear stress was short (<5 s), indicating faster recovery. Upon examination of the G' value for κCA, we believe that the secondary intermolecular bonds between polymer chains were unable to fully reform after subjection to multiple cycles of high strain. Alternatively, the addition of nSi resulted in fast reversible interactions between polymers and nanoparticles. These interactions could be due to the −OH groups of κCA interacting with the nanosilicate's surface.[50] This is important for bioprinting because constructs are not fabricated using continuous extrusions; instead, bioinks are either quickly extruded and subjected to shear or held at rest, depending on if material deposition is required or not. Though bioinks loaded with nSi had lower storage moduli than κCA alone, recoverability of mechanical characteristics is a more appropriate measure of the material behavior in relation to a dynamic printing environment. It is possible that pure κCA had greater polymer−polymer interactions that were subsequently disrupted by nanosilicate inclusion.

Thermo-Reversible Characteristics of κCA−Nanosilicate Bioinks. Pure κCA could not be printed; however, the addition of nSi to κCA allowed printing of 3D structures with high shape fidelity and resolution. To investigate the underlying interactions, shear rheology was performed on κCA and κCA−nSi. Yield stress is an important parameter for 3D printing as it describes the minimum stress needed for materials to flow. Rheology is a powerful platform to analyze the flow properties

DOI: 10.1021/acsami.7b13602
ACS Appl. Mater. Interfaces 2017, 9, 43449−43458

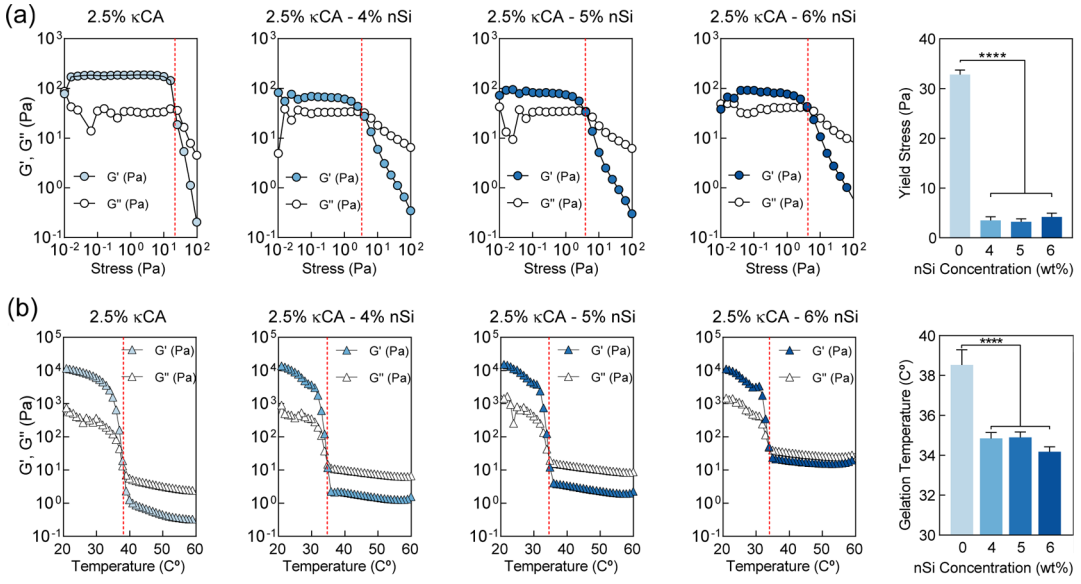

Figure 4. Rheological analysis of κCA−nanosilicate bioinks. (a) Effect of the addition of nSi to κCA on rheological characteristics was monitored using stress sweeps. Storage (G') and loss moduli (G'') were monitored at different shear stresses. Crossover points (yield stress) are shown by dashed red line. Yield stress quantification from stress sweeps reveals a significant decrease in yield stress because of the addition of nSi, resulting in continuous extrusion of the ink. (b) Temperature sweeps (60−20 °C) show the crossover point (gelation point) of bioink compositions. Gelation point analysis shows that in the physiological viable temperature range of 37−40 °C, κCA on its own cannot be printed because of premature gelation. The addition of nSi allows those compositions to be printed at 37 °C and above.

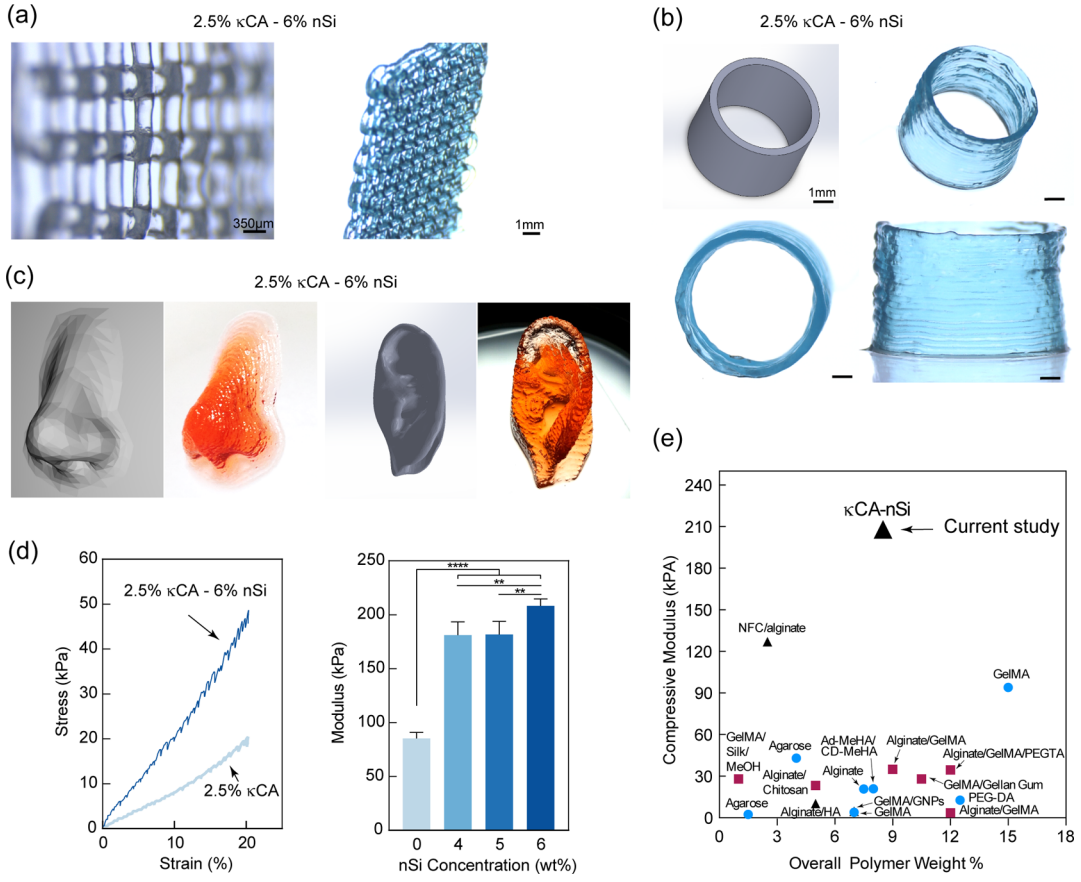

Figure 5. Printing complex structures using κCA−nanosilicate bioinks. (a) κCA−nanosilicate bioinks are capable of printing complex constructs such as a single fiber in a lattice network and a layered lattice network. (b) A 30-layer cylinder printed using the κCA−nanosilicate bioink demonstrate high printability of optimized bioink formulations. (c) Printed anatomically relevant nose and ear display mechanical integrity of κCA−nanosilicate bioinks after 3D printing. (d) Mechanical characterization of the cross-linked κCA−nanosilicate structure displays high mechanical stiffness. (e) In comparison to currently available bioinks, the κCA−nSi bioink has a superior modulus.

DOI: 10.1021/acsami.7b13602
ACS Appl. Mater. Interfaces 2017, 9, 43449−43458

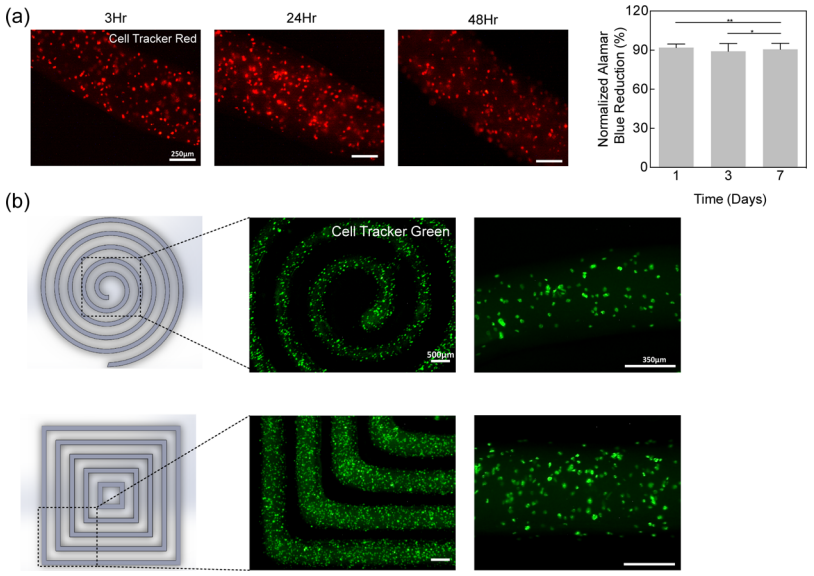

Figure 6. Bioprinted structures using κCA−nanosilicate bioinks. (a) Fluorescent images using CellTracker red showing cells evenly distributed in fibers immediately after 3, 24, and 48 h. alamarBlue assay quantification demonstrating maintained metabolic activity, in printed constructs, for 1, 3, and 7 days. (b) Fluorescent images using CellTracker green, revealing cell distribution in large patterned constructs.

of a material, especially the properties of a bioink. κCA forms random coils because of hydrogen bonding between galactose units when at rest, as it reduces the free energy within the structure. When subjected to a low stress environment, analogous to being held in the barrel without extrusion, κCA polymer chains remain in a random coil configuration. With increasing stress beyond the linear viscoelastic region, crossover of G' and G'' was observed, indicating network yielding. The yield stress point (also known as the crossover point) is reached when the applied shear stress exceeds the attractive force caused by secondary intermolecular bonds (such as the hydrogen bond) within the physically cross-linked network. The effect of nSi on yield stress of bioinks was determined using shear stress sweeps. κCA had a yield stress of 33 ± 1 Pa, while the addition of 6% nSi reduced the yield stress to 4.2 ± 0.76 Pa (Figure 4a). This yield stress indicates the force needed to allow the material to flow. In pure κCA solutions, the hydrogen bonds between polymer strands and junctions are strong, which is reflected in the higher yield stress. However, the addition of nSi results in lower yield stress because of its ability to disrupt polymer−polymer entanglements and improves reversible physical interactions between polymer−nSi.

Amplitude stress sweeps determine yield stress under isothermal conditions (40 °C). However, above the gelation temperature, κCA polymer chains are in a random coil conformation that changes to a double-helix conformation when the temperature is lowered below the gelation point. These double helices are stabilized by hydrogen bonding between anhydrous galactose units in the κCA polymer chain. In this study's printing setup, the material was printed at 35−40 °C onto a 25 °C print bed. For a successful print to occur, the bioink should not thermo-reversibly gel at or close to 37 °C. To simulate this and evaluate the effect of nanosilicate addition on the gelation temperature of the bioink compositions, temperature sweeps were performed from 60 to 20 °C (Figure 4b). Pure κCA gelled close to 40 °C which translated to nonprintable ink. However, nanosilicate compositions had significantly lower gelation temperatures, around 35 °C, which exhibited high shape retention when 3D printing. We believe that the addition of nSi disrupts the hydrogen bonding between κCA polymer chains, which allows the double helices to form, lowering the gelation point of the material. This disruption could stem from the nanosilicate potential to form hydrogen bonds with κCA, taking away some of the κCA polymer chain's ability to interact with itself.[51−53] From these results, it is observed that at least 4% of nSi need to be added to 2.5% κCA to obtain a printable bioink. As proof-of-principle, we selected 2.5% κCA−6 wt % nanosilicate composition for 3D printing. This is mostly due to its high printability, shape fidelity, and physiologically relevant gelation temperature.

3D Printing Complex Structure Using κCA−Nanosilicate Bioinks. One of the primary goals of 3D bioprinting is to print a complex organ or organ system.[54,55] However, current bioinks lack the mechanical strength as well as printability to print larger, mesoscale architectures. To demonstrate the κCA−nanosilicate bioink's ability to print complex shapes with high shape fidelity, we printed a variety of constructs (Figure 5a). Different lattice structures were printed to showcase the shape fidelity and high resolution of the 2.5% κCA−6% nanosilicate bioink (Figure 5a). Large as well as small lattices were printed without compromising lattice porosity. The κCA−nanosilicate bioinks have the ability to print large overhangs and support multiple layers. To mimic more complex architectures, a bioink must be able to print with rounded edges; this was observed by printing a high-aspect-ratio cylinder (Figure 5b). This printed cylinder reveals high shape retention, even under the load of many successive layers (∼30 layers), which is difficult to achieve using softer bioinks. The high stiffness of κCA−nanosilicate bioinks and rapid thermo-reversible gelation allowed multilayered constructs to be printed without collapsing. Importantly, this makes a stable structure that can then be ionically cross-linked without the need for added complexity of support baths or UV radiation. The κCA−nanosilicate bioinks can also print self-supporting anatomical-size structures such as nose and ear without ionic cross-linking (Figure 5c).

After printing, the structure can be cross-linked using potassium ions (K^+) to obtain a mechanically resilient structure.

DOI: 10.1021/acsami.7b13602
ACS Appl. Mater. Interfaces 2017, 9, 43449−43458

We evaluated the effect of the nanosilicate addition to κCA on mechanical properties of cross-linked nanocomposites using uniaxial compression. Nanocomposite gels were fabricated by pouring precursor solution into molds, and once the solutions thermo-reversibly gel, potassium chloride (KCL) was added for ionic cross-linking. There was a significant increase in the mechanical properties of the hydrogels because of the nanosilicate addition (Figure 5d). Compressive modulus for pure 2.5 wt % κCA gels was 85 ± 5.7 kPa, while the addition of 6 wt % nSi resulted in an almost 2.5-fold increase to 208 ± 6.5 kPa. The mechanical properties of κCA−nanosilicate hydrogels are similar to some of the tissues that are subjected to mechanical stress such as cartilage and blood vessels. To our knowledge, available bioinks lack sufficient mechanical strength and are not able to match the physiologically relevant mechanical stiffness. To demonstrate this aspect, we identified and compared moduli of available bioinks with κCA−nanosilicate formulations (Figure 5e). Specifically, we compared three major classifications of bioinks: polymers, polymer blends, and nanocomposites. Single polymer bioinks include agarose,[13,14] alginate,[7,8] GelMA,[9,10] and PEG-DA;[11] polymer blends consist of alginate/chitosan,[56] GelMa/gellan gum,[18] alginate/GelMA,[19] alginate/GelMA/PEGTA,[15] and GelMA/silk/MeOH;[57] and nanocomposites consist of alginate/hydroxyapatite,[58] GelMa/gold nanoparticles, and nanocellulose (NFC)/alginate.[45,59] The κCA−nanosilicate bioink had a higher modulus (208 ± 6.5 kPa) than all presented bioinks. There was not a noticeable difference between bioinks with a single polymer compared to polymer blends, though nanocomposites did appear to be the strongest group. The κCA−nanosilicate bioink has a definite advantage in terms of mechanical characteristics when considering it is in the middle of the range of bioinks for overall polymer weight percentage and is only physically cross-linked. This comparison shows the bioink strength and uniqueness as a novel bioink.

3D Bioprinting Using κCA−Nanosilicate Bioinks. Incorporation of cells into a bioink and ensuring their viability during printing is imperative to a successful bioink.[28] Because of the strong autofluorescence of the bioink and the ability of nSi to adsorb fluorescent dyes, cells were stained with CellTracker green or red prior to loading into the bioink to visualize the distribution of cells within the printed structure (Figure 6a). Often, the process of loading and mixing cells into viscous bioinks can be difficult, but due to the shear-thinning characteristics of κCA−nanosilicate bioinks, cells mixed with the bioink evenly without any aggregation. Finally, an Alamar Blue assay was performed to measure the cell metabolic activity of encapsulated cells. The mean cell metabolic activity of the cells at days 1, 3, and 7 was similar, and no significant difference was observed, indicating that cells maintained viability over time (Figure 6b). Other bioinks such as HA[12] and alginate/nanocellulose[45] revealed similar cell survival on days 5 and 7. Because of a lack of cell-adhesive sites on the κCA backbone, limited cell proliferation was observed. This limitation can be overcome by incorporating cell-binding domains or combining with cell-adhesive polymers. Overall, this study introduces κCA-based hydrogels for bioprinting because of the shear-thinning ability and low yield stress of bioink formulation. In addition, these data also indicate that a 3D-printed structure remains stable over a period of 7 days, without significant degradation/dissolution at physiological conditions.

CONCLUSION

Rapidly gelling, self-supporting bioinks from a natural polymer (κCA) reinforced with 2D nanoparticles (nanosilicate) are introduced. The κCA−nanosilicate bioinks have shear-thinning characteristics and physiologically relevant gelation temperature. Strong interactions between κCA and nSi result in enhanced physical interactions leading to high shape fidelity of printed filament and structural integrity of printed structure. After ionic cross-linking with potassium ions, κCA−nSi result in mechanically stiff hydrogels that can be used to print tissue that undergo constant mechanical load such as cartilage and blood vessels. Because of shear-thinning characteristics, high cell viability was observed in printed cells. In addition, the printed cells retained metabolic activity, indicating the ability of κCA−nanosilicate bioinks to support long-term cultures. Due to lack of cell-binding domains, limited cell spreading was observed, and thus κCA−nanosilicate bioinks can be used to print non-adherent cells such as chondrocytes. By incorporating cell-binding domains or polymer within bioink formulations, cell spreading and proliferation can be obtained. Moreover, the κCA−nanosilicate bioink is also sensitive to temperature changes and below its gelation temperature becomes unprintable. This necessitates precise control of temperature when handling and printing the material. Overall, κCA−nanosilicate bioinks have high shape retention, structural fidelity, and mechanical strength that can be used to print complex physiologically relevant tissues.

MATERIALS AND METHODS

Synthesis and Fabrication of Bioinks. Nanosilicates (Laponite XLS, BYK-Chemie GmbH, Wesel, Germany) were slowly added to diH_2O and vigorously mixed using a magnetic stir rod for 30 min until the initially opaque solution turned clear, indicating that nSi were exfoliated. For the screening of bioinks, the nanosilicate suspensions were heated to desired temperatures (25, 40, or 80 °C), and κCA (Tokyo Chemical Industries, Japan) was slowly added and thoroughly mixed via a magnetic stir bar for 30 additional minutes. Subsequently, solutions were cooled to either 60 or 40 °C. After the ink composition was established, solutions were mixed at 80 °C and then cooled to 40 °C in an oven. Using these processes, κCA/XLS formulations were created using different wt % for each component of the bioink. For all testing and printing, solutions were placed in an oven at the desired temperature (25−60 °C) and utilized when the temperature of the solution reached the desired temperature.

Printability Tests. Printability tests were performed by filling 3 mL syringes with bioinks at specified temperatures and then loading onto an NE-1000 syringe pump (East Farmingdale, New York). The syringes were fitted with a 23-gauge blunt-tipped stainless-steel needle (Jensen Global Inc, Santa Barbara, CA) and extruded with a 0.3 mL/h flow rate. The pump-syringe apparatus was tilted 45° and extruded onto a glass slide.

3D Printing Process. A HYREL System 30M 3D printer (Hyrel L.L.C., Norcross, GA) was used for printing all constructs. Ink compositions were loaded into a VOL-25 extruder cartridge (Hyrel L.L.C., Norcross, GA) at 40 °C equipped with a 23-gauge blunt-tipped stainless-steel needle. STL files were generated from 3D CAD drawings created in SolidWorks and converted to G-code using Slic3r. G-code files were then input into Hyrel's proprietary software (Repetrel) which controlled the printer and print parameters. Unless otherwise specified, prints were performed with the following parameters: a print head speed of 4 mm/s, the nozzle height from the print surface of 350 μm, and a flow rate of 0.3 mL/h. Constructs were printed onto glass slides. After printing, the constructs were cross-linked with 5 wt % KCL for 5 min before being moved into a 10× PBS (phosphate-buffered saline) solution. Constructs were dyed with food coloring and imaged using a stereomicroscope (SteREO

DOI: 10.1021/acsami.7b13602
ACS Appl. Mater. Interfaces 2017, 9, 43449−43458

Discovery.V8, Carl Zeiss Meditec AG, Oberkochen, Germany). Images were processed and analyzed in ImageJ to quantify the fiber size.

Rheological Analysis. All rheological testing was performed with a stress-controlled rheometer (DHR-2 discovery hybrid rheometer, TA Instruments, New Castle, Delaware) using 40 mm parallel plate geometry at a gap of 0.2 mm in conjunction with a solvent trap. Unless noted, all tests were completed at 40 °C to replicate process parameters. To evaluate recoverability of the material, oscillatory time sweeps were performed in 60 s intervals at alternating 100 and 1% strains performed at 1 Hz. Flow rate sweeps were run with a shear rate from 10^{-3} to 10^{3} s^{-1}. To measure yield stress, oscillation stress sweeps were performed at 1 Hz from 10^{-2} to 10^{3} Pa and assessed, where G'' became greater than G'. Finally, temperature sweeps were conducted from 60 to 20 °C at a frequency of 1 Hz and a stress of 10 Pa to observe temperature-induced gelation.

Mechanical Testing. To determine the modulus of the material, cyclic compression testing was performed with an ADMET eXpert 7600 single column testing system (ADMET, Inc., Norwood, Massachusetts) fitted with a 25 lb load cell. Testing was implemented at 20% compression and a strain rate of 10 mm/min. Sample preparation was completed by pouring liquid bioinks into a glass Petri dish and cooling to room temperature. These samples were punched out with a 7 mm punch and placed into 5 wt % KCL for 5 min before being moved into a 10× PBS solution for 1 h. The samples were then gently blotted to remove excess water.

3D Bioprinting and Cell Viability. Inks for cell incorporation were fabricated as previously described (composition: 2.5 wt % κCA and 6 wt % XLS). MC3T3-E1 mouse preosteoblasts (ATCC, Manassas, Virginia) were cultured in alpha-modified minimal essential medium (HyClone) supplemented with 10% fetal bovine serum (Atlanta Biologicals) and 1% penicillin/streptomycin (100 U/100 μg/mL, Gibco). For alamarBlue cell viability assay, cells reached 80% confluency, passaged, and resuspended in inks. The cell-laden ink was loaded and printed as previously described onto glass slides. Constructs were then cross-linked with KCL for 5 min, rinsed with 10× PBS, placed into 12-well plates with culture media, and incubated at 37 °C until further analysis. alamarBlue assay was performed at 1, 3, and 7 days to quantify cell metabolic activity within the printed structures over time. Metabolic activity was normalized to cells seeded on tissue culture plastic. To visualize cells encapsulated within bioinks, cells were incubated at 37 °C with 2 μM CellTracker red or green dye (Thermo Fisher) in 1× PBS for 30 min prior to passaging. Cell imaging was performed using a (Nikon, TE2000-S) fluorescent microscope at 3, 24, and 48 h after encapsulation.

AUTHOR INFORMATION

Corresponding Author

*E-mail: gaharwar@tamu.edu. Phone: 979-458-5540. Fax: 979-845-4450.

ORCID

Akhilesh K. Gaharwar: 0000-0002-0284-0201

Author Contributions

The manuscript was written through contributions of all authors. All authors have given approval to the final version of the manuscript.

Funding

Research reported in this publication was supported by the National Institute Of Biomedical Imaging and Bioengineering (NIBIB) of the National Institutes of Health (NIH) under award no. DP2EB026265 and R03EB02345 and the National Science Foundation (NSF) under award no. CBET 1705852. The content is solely the responsibility of the authors and does not necessarily represent the official views of the National Institutes of Health.

Notes

The authors declare no competing financial interest.

ABBREVIATIONS

ECM, extracellular matrix; G', storage modulus; G'', loss modulus; GelMA, gelatin methacrylate; HA, hyaluronic acid; IPNs, interpenetrating networks; K^+, potassium; κCA, kappa-carrageenan; nSi, nanosilicates or Laponite XLS; PEO/G, poly(ethylene oxide/glycol); RGD, arginyl-glycyl-aspartic acid; XLG, Laponite XLG

REFERENCES

(1) Guvendiren, M.; Lu, H. D.; Burdick, J. A. Shear-thinning hydrogels for biomedical applications. *Soft Matter* **2012**, *8*, 260−272.

(2) Loebel, C.; Rodell, C. B.; Chen, M. H.; Burdick, J. A. Shear-thinning and self-healing hydrogels as injectable therapeutics and for 3D-printing. *Nat. Protoc.* **2017**, *12*, 1521−1541.

(3) Gaharwar, A. K.; Peppas, N. A.; Khademhosseini, A. Nanocomposite hydrogels for biomedical applications. *Biotechnol. Bioeng.* **2014**, *111*, 441−453.

(4) Chimene, D.; Lennox, K. K.; Kaunas, R. R.; Gaharwar, A. K. Advanced Bioinks for 3D Printing: A Materials Science Perspective. *Ann. Biomed. Eng.* **2016**, *44*, 2090−2102.

(5) Zhu, W.; Ma, X.; Gou, M.; Mei, D.; Zhang, K.; Chen, S. 3D printing of functional biomaterials for tissue engineering. *Curr. Opin. Biotechnol.* **2016**, *40*, 103−112.

(6) Gaharwar, A. K.; Arpanaei, A.; Andresen, T. L.; Dolatshahi-Pirouz, A. 3D Biomaterial Microarrays for Regenerative Medicine: Current State-of-the-Art, Emerging Directions and Future Trends. *Adv. Mater.* **2016**, *28*, 771−781.

(7) Ahn, S.; Lee, H.; Puetzer, J.; Bonassar, L. J.; Kim, G. Fabrication of cell-laden three-dimensional alginate-scaffolds with an aerosol cross-linking process. *J. Mater. Chem.* **2012**, *22*, 18735−18740.

(8) Tabriz, A. G.; Hermida, M. A.; Leslie, N. R.; Shu, W. Three-dimensional bioprinting of complex cell laden alginate hydrogel structures. *Biofabrication* **2015**, *7*, 045012.

(9) Schuurman, W.; Levett, P. A.; Pot, M. W.; van Weeren, P. R.; Dhert, W. J. A.; Hutmacher, D. W.; Melchels, F. P. W.; Klein, T. J.; Malda, J. Gelatin-Methacrylamide Hydrogels as Potential Biomaterials for Fabrication of Tissue-Engineered Cartilage Constructs. *Macromol. Biosci.* **2013**, *13*, 551−561.

(10) Bertassoni, L. E.; Cardoso, J. C.; Manoharan, V.; Cristino, A. L.; Bhise, N. S.; Araujo, W. A.; Zorlutuna, P.; Vrana, N. E.; Ghaemmaghami, A. M.; Dokmeci, M. R.; Khademhosseini, A. Direct-write bioprinting of cell-laden methacrylated gelatin hydrogels. *Biofabrication* **2014**, *6*, 024105.

(11) Hockaday, L. A.; Kang, K. H.; Colangelo, N. W.; Cheung, P. Y. C.; Duan, B.; Malone, E.; Wu, J.; Girardi, L. N.; Bonassar, L. J.; Lipson, H.; Chu, C. C.; Butcher, J. T. Rapid 3D printing of anatomically accurate and mechanically heterogeneous aortic valve hydrogel scaffolds. *Biofabrication* **2012**, *4*, 035005.

(12) Ouyang, L.; Highley, C. B.; Rodell, C. B.; Sun, W.; Burdick, J. A. 3D Printing of Shear-Thinning Hyaluronic Acid Hydrogels with Secondary Cross-Linking. *ACS Biomater. Sci. Eng.* **2016**, *2*, 1743−1751.

(13) De Maria, C.; Rincon, J.; Duarte, A. A.; Vozzi, G.; Boland, T. A new approach to fabricate agarose microstructures. *Polym. Adv. Technol.* **2013**, *24*, 895−902.

(14) Campos, D. F. D.; Blaeser, A.; Weber, M.; Jäkel, J.; Neuss, S.; Jahnen-Dechent, W.; Fischer, H. Three-dimensional printing of stem cell-laden hydrogels submerged in a hydrophobic high-density fluid. *Biofabrication* **2013**, *5*, 015003.

(15) Jia, W.; Gungor-Ozkerim, P. S.; Zhang, Y. S.; Yue, K.; Zhu, K.; Liu, W.; Pi, Q.; Byambaa, B.; Dokmeci, M. R.; Shin, S. R.; Khademhosseini, A. Direct 3D bioprinting of perfusable vascular constructs using a blend bioink. *Biomaterials* **2016**, *106*, 58−68.

(16) Colosi, C.; Shin, S. R.; Manoharan, V.; Massa, S.; Costantini, M.; Barbetta, A.; Dokmeci, M. R.; Dentini, M.; Khademhosseini, A. Microfluidic Bioprinting of Heterogeneous 3D Tissue Constructs Using Low-Viscosity Bioink. *Adv. Mater.* **2016**, *28*, 677−684.

(17) Pati, F.; Jang, J.; Ha, D.-H.; Kim, S. W.; Rhie, J.-W.; Shim, J.-H.; Kim, D.-H.; Cho, D.-W. Printing three-dimensional tissue analogues

DOI: 10.1021/acsami.7b13602
ACS Appl. Mater. Interfaces 2017, 9, 43449−43458

with decellularized extracellular matrix bioink. *Nat. Commun.* **2014**, *5*, 3935.
(18) Melchels, F. P. W.; Dhert, W. J. A.; Hutmacher, D. W.; Malda, J. Development and characterisation of a new bioink for additive tissue manufacturing. *J. Mater. Chem. B* **2014**, *2*, 2282−2289.
(19) Chung, J. H. J.; Naficy, S.; Yue, Z.; Kapsa, R.; Quigley, A.; Moulton, S. E.; Wallace, G. G. Bio-ink properties and printability for extrusion printing living cells. *Biomater. Sci.* **2013**, *1*, 763−773.
(20) Kolesky, D. B.; Homan, K. A.; Skylar-Scott, M. A.; Lewis, J. A. Three-dimensional bioprinting of thick vascularized tissues. *Proc. Natl. Acad. Sci. U. S. A.* **2016**, *113*, 3179−3184.
(21) Barry, R. A.; Shepherd, R. F.; Hanson, J. N.; Nuzzo, R. G.; Wiltzius, P.; Lewis, J. A. Direct-Write Assembly of 3D Hydrogel Scaffolds for Guided Cell Growth. *Adv. Mater.* **2009**, *21*, 2407−2410.
(22) Tekin, H.; Sanchez, J. G.; Landeros, C.; Dubbin, K.; Langer, R.; Khademhosseini, A. Controlling Spatial Organization of Multiple Cell Types in Defined 3D Geometries. *Adv. Mater.* **2012**, *24*, 5543−5547.
(23) Jia, J.; Richards, D. J.; Pollard, S.; Tan, Y.; Rodriguez, J.; Visconti, R. P.; Trusk, T. C.; Yost, M. J.; Yao, H.; Markwald, R. R.; Mei, Y. Engineering alginate as bioink for bioprinting. *Acta Biomater.* **2014**, *10*, 4323−4331.
(24) Wu, Z.; Su, X.; Xu, Y.; Kong, B.; Sun, W.; Mi, S. Bioprinting three-dimensional cell-laden tissue constructs with controllable degradation. *Sci. Rep.* **2016**, *6*, 24474.
(25) Duan, B. State-of-the-Art Review of 3D Bioprinting for Cardiovascular Tissue Engineering. *Ann. Biomed. Eng.* **2016**, *45*, 195−209.
(26) Hospodiuk, M.; Dey, M.; Sosnoski, D.; Ozbolat, I. T. The bioink: A comprehensive review on bioprintable materials. *Biotechnol. Adv.* **2017**, *35*, 217−239.
(27) Billiet, T.; Vandenhaute, M.; Schelfhout, J.; Van Vlierberghe, S.; Dubruel, P. A review of trends and limitations in hydrogel-rapid prototyping for tissue engineering. *Biomaterials* **2012**, *33*, 6020−6041.
(28) Ozbolat, I. T.; Hospodiuk, M. Current advances and future perspectives in extrusion-based bioprinting. *Biomaterials* **2016**, *76*, 321−343.
(29) Forget, A.; Blaeser, A.; Miessmer, F.; Köpf, M.; Campos, D. F. D.; Voelcker, N. H.; Blencowe, A.; Fischer, H.; Shastri, V. P. Mechanically Tunable Bioink for 3D Bioprinting of Human Cells. *Adv. Healthcare Mater.* **2017**, *6*, 1700255.
(30) Gasperini, L.; Mano, J. F.; Reis, R. L. Natural polymers for the microencapsulation of cells. *J. R. Soc., Interface* **2014**, *11*, 20140817.
(31) Popa, E. G.; Carvalho, P. P.; Dias, A. F.; Santos, T. C.; Santo, V. E.; Marques, A. P.; Viegas, C. A.; Dias, I. R.; Gomes, M. E.; Reis, R. L. Evaluation of the in vitro and in vivo biocompatibility of carrageenan-based hydrogels. *J. Biomed. Mater. Res., Part A* **2014**, *102*, 4087−4097.
(32) Nishinari, K.; Watase, M. Effects of sugars and polyols on the gel-sol transition of kappa-carrageenan gels. *Thermochim. Acta* **1992**, *206*, 149−162.
(33) Tecante, A.; del Carmen Núñez Santiago, M. Solution properties of κ-carrageenan and its interaction with other polysaccharides in aqueous media. *Rheology*; De Vicente, J., Ed.; InTech, 2012.
(34) Hermansson, A.-M.; Eriksson, E.; Jordansson, E. Effects of potassium, sodium and calcium on the microstructure and rheological behaviour of kappa-carrageenan gels. *Carbohydr. Polym.* **1991**, *16*, 297−320.
(35) Dawson, J. I.; Oreffo, R. O. C. Clay: New Opportunities for Tissue Regeneration and Biomaterial Design. *Adv. Mater.* **2013**, *25*, 4069−4086.
(36) Chimene, D.; Alge, D. L.; Gaharwar, A. K. Two-Dimensional Nanomaterials for Biomedical Applications: Emerging Trends and Future Prospects. *Adv. Mater.* **2015**, *27*, 7261−7284.
(37) Xavier, J. R.; Thakur, T.; Desai, P.; Jaiswal, M. K.; Sears, N.; Cosgriff-Hernandez, E.; Kaunas, R.; Gaharwar, A. K. Bioactive nanoengineered hydrogels for bone tissue engineering: a growth-factor-free approach. *ACS Nano* **2015**, *9*, 3109−3118.
(38) Thakur, A.; Jaiswal, M. K.; Peak, C. W.; Carrow, J. K.; Gentry, J.; Dolatshahi-Pirouz, A.; Gaharwar, A. K. Injectable shear-thinning nanoengineered hydrogels for stem cell delivery. *Nanoscale* **2016**, *8*, 12362−12372.
(39) Cross, L. M.; Shah, K.; Palani, S.; Peak, C. W.; Gaharwar, A. K. Gradient nanocomposite hydrogels for interface tissue engineering. *Nanomedicine* **2017**, DOI: 10.1016/j.nano.2017.02.022.
(40) Peak, C. W.; Stein, J.; Gold, K. A.; Gaharwar, A. K. Nanoengineered Colloidal Inks for 3D Bioprinting. *Langmuir* **2017**, DOI: 10.1021/acs.langmuir.7b02540.
(41) Peak, C. W.; Carrow, J. K.; Thakur, A.; Singh, A.; Gaharwar, A. K. Elastomeric Cell-Laden Nanocomposite Microfibers for Engineering Complex Tissues. *Cell. Mol. Bioeng.* **2015**, *8*, 404−415.
(42) Paul, A.; Manoharan, V.; Krafft, D.; Assmann, A.; Uquillas, J. A.; Shin, S. R.; Hasan, A.; Hussain, M. A.; Memic, A.; Gaharwar, A. K.; Khademhosseini, A. Nanoengineered Biomimetic Hydrogels for Guiding Human Stem Cell Osteogenesis in Three Dimensional Microenvironments. *J. Mater. Chem. B* **2016**, *4*, 3544−3554.
(43) Liu, S.; Chan, W. L.; Li, L. Rheological properties and scaling laws of κ-carrageenan in aqueous solution. *Macromolecules* **2015**, *48*, 7649−7657.
(44) Panwar, A.; Tan, L. Current Status of Bioinks for Micro-Extrusion-Based 3D Bioprinting. *Molecules* **2016**, *21*, 685.
(45) Markstedt, K.; Mantas, A.; Tournier, I.; Ávila, H. M.; Hägg, D.; Gatenholm, P. 3D Bioprinting Human Chondrocytes with Nanocellulose−Alginate Bioink for Cartilage Tissue Engineering Applications. *Biomacromolecules* **2015**, *16*, 1489−1496.
(46) He, Y.; Yang, F.; Zhao, H.; Gao, Q.; Xia, B.; Fu, J. Research on the printability of hydrogels in 3D bioprinting. *Sci. Rep.* **2016**, *6*, 29977.
(47) Rezende, R. A.; Bártolo, P. J.; Mendes, A.; Filho, R. M. Rheological behavior of alginate solutions for biomanufacturing. *J. Appl. Polym. Sci.* **2009**, *113*, 3866−3871.
(48) Belalia, F.; Djelali, N.-E. Rheological properties of sodium alginate solutions. *Rev. Roum. Chim.* **2014**, *59*, 135−145.
(49) Blaeser, A.; Campos, D. F. D.; Puster, U.; Richtering, W.; Stevens, M. M.; Fischer, H. Controlling Shear Stress in 3D Bioprinting is a Key Factor to Balance Printing Resolution and Stem Cell Integrity. *Adv. Healthcare Mater.* **2016**, *5*, 326−333.
(50) El Adraa, K.; Timon, V.; Lambert, J.-F.; Al-Rabaa, A.-R.; Jaber, F.; Jaber, M.; Tielens, F. Adsorption of l-DOPA Intercalated in Hydrated Na-Saponite Clay: A Combined Experimental and Theoretical Study. *J. Phys. Chem. C* **2012**, *116*, 26414−26421.
(51) Haraguchi, K. Synthesis and properties of soft nanocomposite materials with novel organic/inorganic network structures. *Polym. J.* **2011**, *43*, 223−241.
(52) Haraguchi, K.; Li, H.-J.; Matsuda, K.; Takehisa, T.; Elliott, E. Mechanism of Forming Organic/Inorganic Network Structures during In-situ Free-Radical Polymerization in PNIPA−Clay Nanocomposite Hydrogels. *Macromolecules* **2005**, *38*, 3482−3490.
(53) Haraguchi, K.; Farnworth, R.; Ohbayashi, A.; Takehisa, T. Compositional Effects on Mechanical Properties of Nanocomposite Hydrogels Composed of Poly(N,N-dimethylacrylamide) and Clay. *Macromolecules* **2003**, *36*, 5732−5741.
(54) Murphy, S. V.; Atala, A. 3D bioprinting of tissues and organs. *Nat. Biotechnol.* **2014**, *32*, 773−785.
(55) Radhakrishnan, J.; Subramanian, A.; Krishnan, U. M.; Sethuraman, S. Injectable and 3D Bioprinted Polysaccharide Hydrogels: From Cartilage to Osteochondral Tissue Engineering. *Biomacromolecules* **2017**, *18*, 1−26.
(56) Colosi, C.; Costantini, M.; Latini, R.; Ciccarelli, S.; Stampella, A.; Barbetta, A.; Massimi, M.; Devirgiliis, L. C.; Dentini, M. Rapid prototyping of chitosan-coated alginate scaffolds through the use of a 3D fiber deposition technique. *J. Mater. Chem. B* **2014**, *2*, 6779−6791.
(57) Xiao, W.; He, J.; Nichol, J. W.; Wang, L.; Hutson, C. B.; Wang, B.; Du, Y.; Fan, H.; Khademhosseini, A. Synthesis and characterization of photocrosslinkable gelatin and silk fibroin interpenetrating polymer network hydrogels. *Acta Biomater.* **2011**, *7*, 2384−2393.
(58) Gao, G.; Schilling, A. F.; Yonezawa, T.; Wang, J.; Dai, G.; Cui, X. Bioactive nanoparticles stimulate bone tissue formation in

bioprinted three-dimensional scaffold and human mesenchymal stem cells. *Biotechnol. J.* **2014**, *9*, 1304−1311.
(59) Zhu, K.; Shin, S. R.; van Kempen, T.; Li, Y.-C.; Ponraj, V.; Nasajpour, A.; Mandla, S.; Hu, N.; Liu, X.; Leijten, J.; Lin, Y.-D.; Hussain, M. A.; Zhang, Y. S.; Tamayol, A.; Khademhosseini, A. Gold Nanocomposite Bioink for Printing 3D Cardiac Constructs. *Adv. Funct. Mater.* **2017**, *27*, 1605352.

DOI: 10.1021/acsami.7b13602
ACS Appl. Mater. Interfaces 2017, 9, 43449−43458